IOP Publishing Journal of Physics: Condensed Matter
J. Phys.: Condens. Matter **31** (2019) 495701 (9pp) https://doi.org/10.1088/1361-648X/ab3dd6

Robust generation of half-metallic transport and pure spin current with photogalvanic effect in zigzag silicene nanoribbons

Peng Jiang[1,2], Lili Kang[1,2], Xixi Tao[1,2], Ning Cao[1,2], Hua Hao[1], Xiaohong Zheng[1,2,3], Lei Zhang[3,4] and Zhi Zeng[1,2]

[1] Key Laboratory of Materials Physics, Institute of Solid State Physics, Chinese Academy of Sciences, Hefei 230031, People's Republic of China
[2] University of Science and Technology of China, Hefei 230026, People's Republic of China
[3] State Key Laboratory of Quantum Optics and Quantum Optics Devices, Institute of Laser Spectroscopy, Shanxi University, Taiyuan 030006, People's Republic of China
[4] Collaborative Innovation Center of Extreme Optics, Shanxi University, Taiyuan 030006, People's Republic of China

E-mail: xhzheng@theory.issp.ac.cn and zhanglei@sxu.edu.cn

Received 16 July 2019, revised 7 August 2019
Accepted for publication 22 August 2019
Published 9 September 2019

Abstract

Using first-principles density functional theory combined with non-equilibrium Green's function method, we investigate the spin-dependent current generated by photogalvanic effect (PGE) in photoelectric devices based on zigzag silicence nanoribbons with unsymmetrical sp^2–sp^3 hydrogen passivated edges (H-2H ZSiNRs) and C_s symmetry. Due to their unique atomic structures and spin-semiconductor properties, we find that the flow direction of different spin channels, spin polarization and magnitude of the photocurrent can be efficiently controlled by tuning the photon energy (E_{ph}) or polarization/helicity angle (θ) of the incident polarized light. Interestingly, at certain polarization/helicity angles or certain photon energy, 100% spin polarized current can be achieved by either linearly or elliptically polarized light. Further, robust pure spin current without an accompanying charge current can be achieved by the irradiation of linearly and elliptically polarized light when the two leads are in antiparallel magnetic configuration and $\theta = 0°$, 90° and 180°. Most importantly, without suffering from Schottky barriers or tunnel barriers at metal-semiconductor interfaces, the generated pure spin current or fully spin polarized current in such a purely two-dimensional device with PGE is several orders of magnitude larger than those achieved in metal/semiconductor/metal structures. These numerical results suggest that the asymmetrically sp^2–sp^3 terminated ZSiNRs are promising materials for construction of novel photoinduced pure spin current and fully spin polarized current generators, which will be of great significance in future spintronic applications.

Keywords: spin current, photogalvanic effect, silicene nanoribbon, first-principles

(Some figures may appear in colour only in the online journal)

1. Introduction

Spintronics, which involves encoding and transferring information in memory and logic devices by utilizing the spin degree of freedom of electrons, has drawn great attention due to the great advantages of high operating speed and low energy consumption. The control of spin transport is a basic but crucial task in spintronics and the realization of highly spin polarized transport and pure spin current is particularly important [1–3]. Since the scaling of the traditional electronic devices has almost reached the limitation in semiconductor industry, Si-based two-dimensional (2D) materials emerge as good

candidates for building spintronic devices [4–6]. Silicene [7], a 2D hexagonal atomic structure with small buckling in the two sublattices in the vertical direction, has been synthesized in experiments [4]. Previous studies have shown that, similar to graphene [4, 7], the low-buckled silicene is a zero band-gap semimetal and its bands cross at the Fermi level forming a Dirac cone. Moreover, many fascinating properties, such as spin-filter effect [5, 8], quantum spin Hall effect [9, 10], spin-caloritronic effect [11, 12], etc, have been observed in silicene and its derivatives. Thus, silicene based materials hold great potential for achieving half-metallic (fully spin polarized) transport and pure spin current.

Light irradiation is an effective driving force in the generation of electric current and actually photoinduced electron transport in 2D materials have received special attention in recent years [13–17]. It was generally believed that, in the generation of photocurrent in photoelectric transistors, an auxiliary external bias voltage must be needed to drive the photon-excited electrons towards one direction to achieve a net current. Very interestingly, not long ago, it has been shown that an external bias is not indispensable for the production of photocurrent and it can be well induced by light illuminati on materials lacking space inversion symmetry. This phenomenon is called the photogalvanic effect (PGE) [18]. PGE has now been widely investigated, firstly in bulk systems, such as Tellurium crystals [19] and *p*-GaAs/AlGaAs multiple-quantum wells [20], and then in 2D and 1D systems, such as, WSe_2 [13], S-doped monolayer black phosphorus [14], black phosphorene/blue phosphorene vdWs vertical heterostructure [21] and other nanoribbons [16, 22]. If electrons with different spins can be driven to flow towards opposite directions by PGE, undoubtedly, it will add a new way for spin current generation. Recently, Xie *et al*'s work of generating pure spin current with magnetic tunnel junction based on 2D phosphorene provides a good attempt towards this aim [15].

In this work, we design a spin photogalvanic device based on on zigzag silicence nanoribbons with unsymmetrical sp^2–sp^3 hydrogen passivated edges (H-2H ZSiNRs) and C_s point group, in which the edge Si atoms at one edge are terminated by one H atom (sp^2 hybridization) while those on the other edge are terminated by two H atoms (sp^3 hybridization). Such ZSiNRs were first studied by Ding *et al* [23] and the ground state was found to be a ferromagnetic spin semiconductor [24]. Owing to the broken space inversion symmetry, a finite charge photocurrent is expected by PGE, without the application of an external bias voltage. However, is the photocurrent generated by PGE spin polarized? Can fully spin polarized current and even pure spin current be produced? It is our purpose to answer these questions in this work.

2. Theory and method

The proposed photoelectric device is presented in figures 1(a) and (b), in which an infinite H-2H 6-ZSiNR is divided into three parts: left lead, right lead and central (channel) region. The transport direction is along the z axis and the width of ribbon in the x direction contains six zigzag chains. The left and right leads extend to $\pm\infty$. The relaxed lattice constant of the H-2H ZSiNR along the z direction is 3.86 Å, consistent with previous theoretical studies [23]. Six unit cells are chosen as the central region, thus its length is 23.16 Å. However, in order to get C_s symmetry, the atoms at both boundaries between the leads and the central region are chosen in the central region, thus it contains 96 atoms. This two-probe structure has no spatial inversion symmetry due to unsymmetrical H-termination, but it has mirror symmetry. The photocurrent is generated by linear polarized light (LPL) or EPL shining on all atoms of the whole central region, as shown in figure 1.

According to the theoretical approach for calculating photocurrent by the PGE based on density functional theory (DFT) combined with non-equilibrium Green's function formalism, [25, 26] the photocurrent flowing from the central region to the lead α can be written as [17, 27]

$$I^{\mathrm{ph}}_{\alpha,\sigma} = \frac{\mathrm{i}e}{h}\int T_{\mathrm{eff},\alpha,\sigma}(\varepsilon)\mathrm{d}\varepsilon, \tag{1}$$

where the effective transmission function

$$T_{\mathrm{eff},\alpha,\sigma}(\varepsilon) = \mathrm{Tr}\{\Gamma_{\alpha,\sigma}(\varepsilon)[(1-f_\alpha(\varepsilon))G^{<}_{\mathrm{ph}}(\varepsilon) + f_\alpha(\varepsilon)G^{>}_{\mathrm{ph}}(\varepsilon)]\}. \tag{2}$$

Here, α (L, R) and σ $(\uparrow, \downarrow)$ denote the lead and spin index, respectively. For simplicity, the spin index σ will be omitted from now on. $\Gamma_\alpha = \mathrm{i}(\Sigma^r_\alpha - \Sigma^a_\alpha)$ is the line-width function of the lead α describing the coupling between the central region and lead α and $\Sigma^{r/a}_\alpha$ is the self-energy of the semi-infinite lead α. f_α is the Fermi–Dirac distribution of the lead α. $G^{<(>)}_{\mathrm{ph}} = G^r_0[\Sigma^{<(>)}_{\mathrm{ph}} + \Sigma^{<(>)}_L + \Sigma^{<(>)}_R]G^a_0$ is the lesser (greater) Green's function of the central region with the electron–photon interaction considered in the first-order Born approximation [25]. G^r_0 (G^a_0) is the retarded (advanced) Green's function of the central region without considering the electron–photon interaction. $\Sigma^{</>}_{\mathrm{ph}}$ is the self-energy of the leads with the electron–photon interaction taken into consideration. The self-energy includes the information about the polarization of the polarized light which is characterized by a complex vector $\mathbf{A}$. For LPL, the polarization vector is defined as $\mathbf{A} = \cos(\theta)\mathbf{e_1} + \sin(\theta)\mathbf{e_2}$, where θ is the polarization angle formed by the polarized direction with respect to the vector $\mathbf{e_1}$. In this work, the vectors $\mathbf{e_1}$ and $\mathbf{e_2}$ are set along z and x directions, respectively (see figure 1 in the main text). $\mathbf{e_1} \times \mathbf{e_2}$ determines the propagation direction of the applied polarized light and thus the light is incident along y direction. As for EPL, the polarization vector is defined as $\mathbf{A} = \cos(\theta)\mathbf{e_1} + i\sin(\theta)\mathbf{e_2}$, where θ determines the light's helicity. In particular, $\theta = \pm 45°$ corresponds to the right and left circularly polarized light (CPL), respectively.

Structure relaxation is performed by the Vienna *ab initio* simulation package (VASP) [28, 29], which is based on DFT using the projector-augmented wave method and a plane wave basis set [30]. The generalized gradient approximation (GGA) with form of Perdew–Burke–Ernzerhof (PBE) [31] is adopted

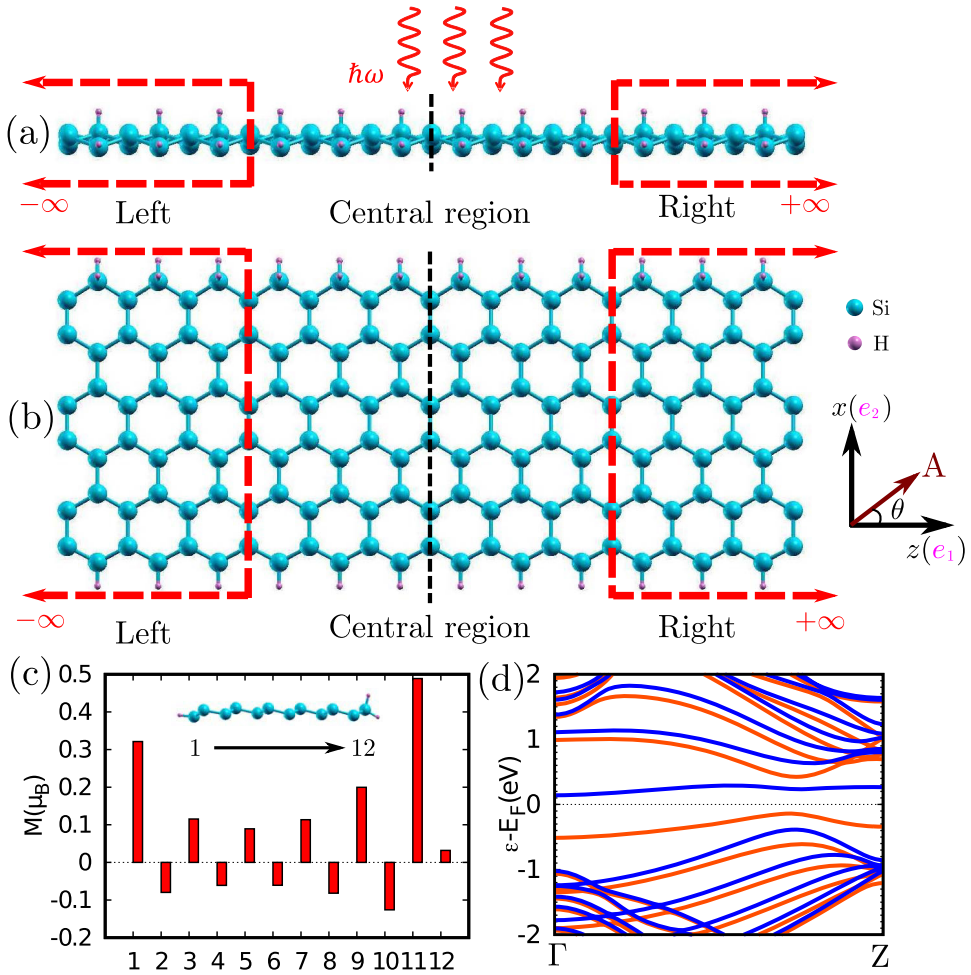

Figure 1. (a) A schematic plot of two-probe photocurrent device with H-2H 6-ZSiNR: (a) side view, (b) top view. The atoms at the boundary between the leads and the central region belongs to the central region so that it has C_s symmetry. The red spiral arrows denote the incident direction of the applied polarized light and $\hbar\omega$ is the incident photon energy. The two polarized vectors $\mathbf{e_1}$ and $\mathbf{e_2}$ define the light propagation direction. $\mathbf{A}$ is the electromagnetic vector potential and θ is the polarization angle for linearly polarized light or helicity angle for elliptically polarized light (EPL). (c) The magnetic moment of Si atoms in one unit cell of H-2H 6-ZSiNR. The inset of figure (c) describes the Si atom indices '$1 \rightarrow 12$' in a unit cell along the x axis. (d) Spin-polarized band structure of H-2H 6-ZSiNR. The red and blue lines denote spin-up and spin-down bands, respectively.

for the exchange-correlation potential. The energy cutoff is set to be 500 eV. The k-point sampling grid is chosen as $1 \times 1 \times 40$. The relaxation process goes on until the residual force on each atom is less than 0.01 eV Å^{-1}.

All transport calculations including the electronic structure and photocurrent are performed by the first-principles software package NanoDcal package [32], which is based on DFT combined with the nonequilibrium Green's function (NEGF) method [32, 33]. The exchange and correlation functional is adopted in the PBE form [31]. Along the y axis, a vacuum region of about 20 Å is applied in order to eliminate the interaction between neighboring images. Norm-conserving pseudopotentials are adopted to describe the atomic cores and linear combinations of atomic orbitals in the double zeta polarized (DZP) form are chosen to expand the electron wave functions. The energy cutoff is set to 200 Ry and the k-point sampling mesh for the lead part of the transport calculation is $1 \times 1 \times 100$.

For convenience, we introduce a spin dependent photoresponse function to represent the normalized photocurrent,

$$R_{\alpha,\sigma} = \frac{I^{\mathrm{ph}}_{\alpha,\sigma}}{eI_\omega} \tag{3}$$

where I_ω is the photon flux defined by the number of photons per unit area per time, thus R has a dimension of area, a_0^2/photon where a_0 is Bohr radius. Based on above definitions, we can define spin current photoresponse function $R_s = R_\uparrow - R_\downarrow$, total charge current photoresponse function $R_c = R_\uparrow + R_\downarrow$, and spin polarization

$$\eta = \left|\frac{R_\uparrow - R_\downarrow}{R_\uparrow + R_\downarrow}\right| \times 100\%, \tag{4}$$

where $R_\uparrow$ and $R_\downarrow$ is not equal to 0 simultaneously. According to the value of η, there are four situations:

(1) When $\eta < 100\%$, the two spin channels flow in the same direction;
(2) When $\eta = 100\%$, the current is 100% spin polarized;
(3) When $\eta > 100\%$, the two spin channels flow in the opposite directions, which means the generation of spin current;

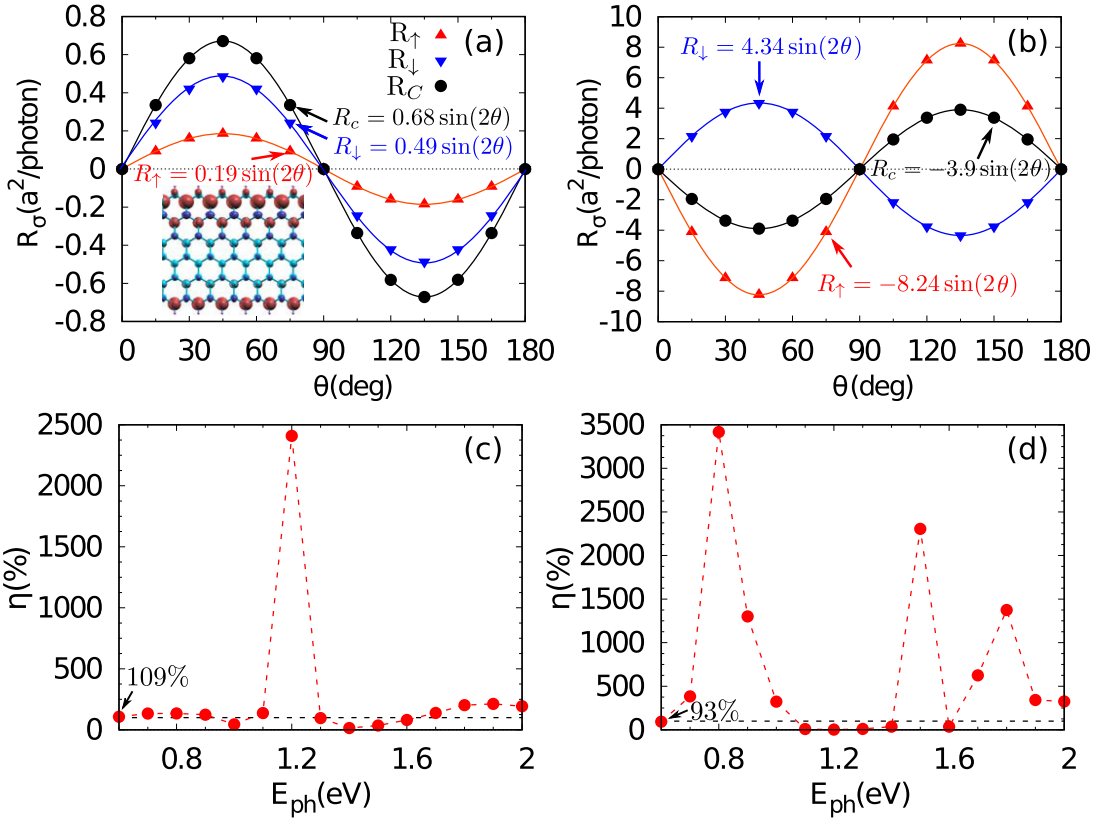

Figure 2. The spin dependent photoresponse and total charge photoresponse as a function of θ under illumination by (a) LPL and (b) EPL with $E_{ph} = 1.0$ eV in configuration 'P'. The spin polarization versus different photon energies is shown (c) for LPL and (d) for EPL. In (c) and (d), the horizontal dashed line marks the position of 100%.

(4) When $\eta \to \infty$, namely, $R_\uparrow + R_\downarrow \to 0$, pure spin current is generated.

In (1) and (2), when $R_\uparrow + R_\downarrow > 0$, the charge current flows to right, otherwise, it flows to left. In (3) and (4), when $R_\uparrow - R_\downarrow > 0$, the spin current flows to right, otherwise, it flows to left.

3. Results and discussion

Before analyzing the PGE, we investigate the electronic structure of the H-2H 6-ZSiNR used for constructing the device. To obtain the most stable magnetic state, we calculate the total energies of the different magnetic configurations, including ferromagnetic (FM), antiferromagnetic (AFM), and nonmagnetic (NM) states. The initial configurations for the FM and AFM are set as follows: for the FM case, the initial magnetic moments of all atoms are set to 0.5 μ_B, while for the AFM case, the initial magnetic moments of half the Si atoms at one edge are set as 0.5 μ_B and those of the other half Si atoms at the other edge are all set as -0.5 μ_B. The numerical results after self-consistence show that the FM state is the lowest in total energy, 20 meV lower than the AFM state and 110 meV lower than the NM state per unit cell, indicating that the FM state is the ground state, thus we only consider the FM ground state in the following transport calculations. Figure 1(c) shows the magnetic moment of the Si atoms in the unit cell. It is found that dihydrogenation greatly suppresses the magnetic moment ($\sim$0.03 μ_B) of the edge sp^3 hybridized Si atom (Si_{12}), whereas the atomic magnetic moment of its nearest Si neighbor (Si_{11}) is 0.49 μ_B, much larger than that ($\sim$0.32 μ_B) of the edge sp^2 hybridized Si atom (Si_1). The increased magnetic moment on Si_{11} results from the formation of an extra π dangling bond due to the sp^3 hybridization on Si_{12}. Namely, since the Si_{12} atom does not contribute to the system-wide π bond due to the sp^3 hybridization, the π bond is terminated between Si_{11} and Si_{12}, thus a π dangling bond is developed on Si_{11}. Our results are well consistent with previous study [23]. The band structure in the FM state is shown in figure 1(d). It indicates that H-2H 6-ZSiNR is a spin-semiconductor, in which there are bipolar spin states around the Fermi level and both spin channels are semiconducting and relatively energy shifted, leading to a spin gap. Meanwhile, the spin-up state has a direct gap 0.57 eV, whereas the spin-down state has an indirect gap 0.53 eV. Actually, our extensive calculations demonstrate that the spin-semiconductor feature is a common one in all the H-2H ZSiNRs, independent of the ribbon width, although the band gap may vary. Next, we will discuss how to utilize H-2H ZSiNR's spin-semiconducting property in two-probe devices to produce fully spin polarized current and pure spin current by PGE.

We consider two magnetic configurations, in which the magnetizations of the two leads are aligned parallel ('P') or anti-parallel ('A'). Firstly, we study the PGE of configuration 'P'. The spin-dependent $R_\sigma(\sigma = \uparrow, \downarrow)$ and charge photoresponse R_c as a function of the polarization or helicity angle θ by the perpendicular illumination of LPL and EPL with

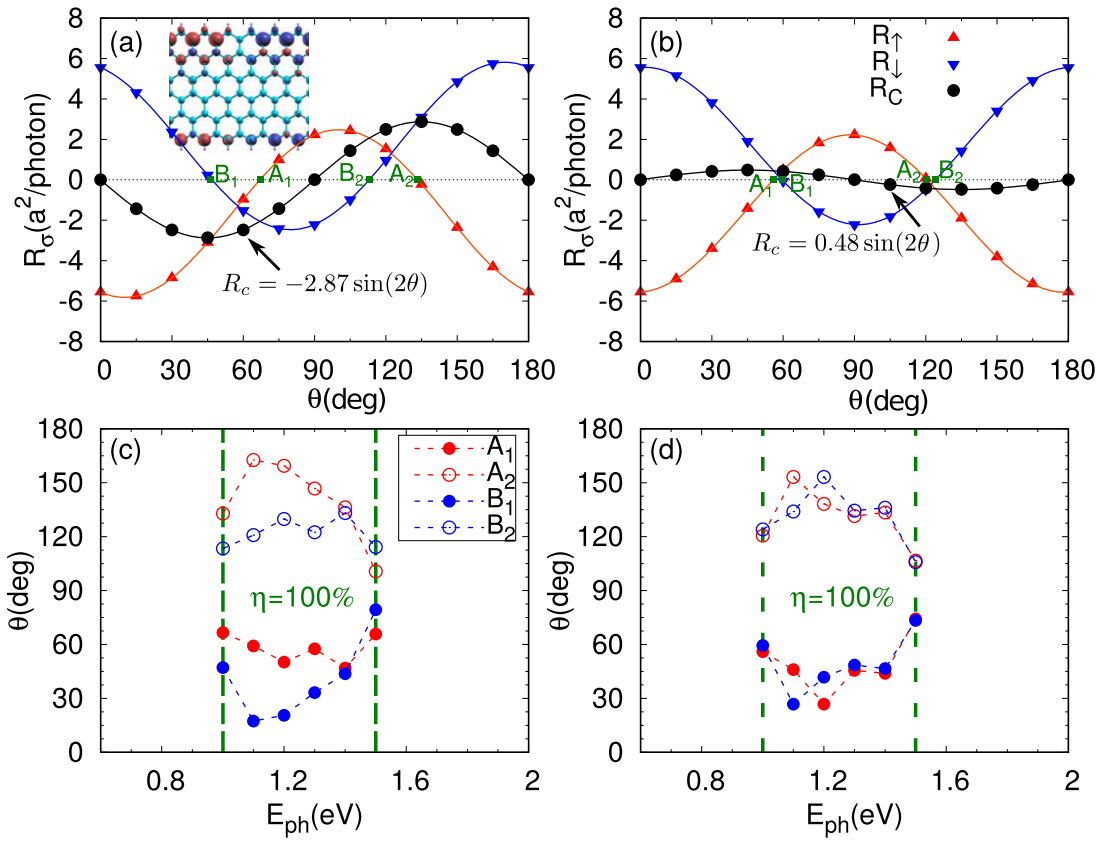

Figure 3. The spin dependent photoresponse and charge photoresponse as a function of θ under (a) LPL and (b) EPL with $E_{ph} = 1.0$ eV in configuration 'A', and the special polarization/helicity angles at which fully spin polarization ($\eta = 100\%$) occurs versus photon energy for (c) LPL and (d) EPL.

$E_{ph} = 1.0$ eV are shown in figures 2(a) and (b), respectively. It is found that both the spin-up photoresponse $R_\uparrow$ and spin-down photoresponse $R_\downarrow$ vary as a function of $\sin(2\theta)$, with the maximum occuring at $\theta = 45°$ or 135°. For example, for LPL, $R_\uparrow$ and $R_\downarrow$ are well fitted by $R_\uparrow = 0.19\sin(2\theta)$ and $R_\downarrow = 0.49\sin(2\theta)$, with the same sign at all polarization angles, thus the total charge photoresponse $R_c = R_\uparrow + R_\downarrow$ also presents the sine dependence on 2θ with $R_c = 0.68\sin(2\theta)$. This sine dependence is a common feature of the linear photogalvanic effect (LPGE) in several systems with C_s symmetry [18]. In contrast, for EPL, it is seen that the signs of $R_\uparrow$ and $R_\downarrow$ are opposite, indicating that the spin-up photocurrent $I^{ph}_\uparrow$ and spin-down photocurrent $I^{ph}_\downarrow$ flow in opposite directions and spin current is generated by elliptic photogalvanic effect (EPGE) at this photon energy. Note that when $\theta = 0°$, 90° and 180°, both the charge current and spin current will be zero for either LPGE or EPGE.

Spin polarization η, as defined by equation (4), is vital for the performance of a spintronic device. Owing to the robust sine dependence of LPL/EPL on the polarization/helicity angle, η will be constant with the change of polarization/helicity angle. Thus, we will focus on the effect of photon energy. We calculate the spin polarization η when $\theta = 45°$ for both LPL and EPL within the photon energy range of [0.6, 2.0] eV as shown in figures 2(c) and (d), respectively. Note that $\theta = \pm 45°$ corresponds to the right and left CPL, respectively. It is seen that η varies rapidly from 14.0% to 2409% for LPL and 2.0% to 3417% for CPL. It crosses the 100% line several times for both cases, which means that with the increase of photon energy, the two spin channels may flow either in the same direction or in opposite directions. Especially, 100% spin polarization can be achieved by tuning the photon energy. Further, we have $\eta = 2409\%$ at $E_{ph} = 1.2$ eV for LPL, and $\eta = 3417\%$ and 2305% at $E_{ph} = 0.8$ and 1.5 eV respectively for CPL. Such huge η means nearly pure spin current is generated.

In the following, the PGE in the device with configuration 'A' is studied. Figures 3(a) and (b) show the spin-dependent photoresponse as a function of θ under the normal illumination of the LPL/EPL with $E_{ph} = 1.0$ eV, respectively. Compared with configuration 'P', both $R_\uparrow$ and $R_\downarrow$ still maintain sine dependence on 2θ, but there are shifts along both the horizontal and longitudinal axes, namely, they vary as $a\sin(2\theta + b) + c$ (see figures 3(a) and (b)). By fitting, we have $R_\uparrow = 4.15\sin(2\theta - 109.48°) - 1.67$ and $R_\downarrow = 4.15\sin(2\theta + 109.48°) + 1.67$ for LPL, and $R_\uparrow = 3.89\sin(2\theta - 86.56°) + 1.67$ and $R_\downarrow = 3.89\sin(2\theta + 86.56°) - 1.67$ for CPL. It indicates that the shifts in both the phase (b) and the amplitude (c) in the two spin channels are exactly opposite to each other and the peak-to-valley difference (a) is exactly the same. It means that if for spin up, $R_\uparrow = a\sin(2\theta + b) + c$, then for spin down, we will have $R_\downarrow = a\sin(2\theta - b) - c$. From this, we can get $R_\uparrow(\theta) = -R_\downarrow(\theta)$ when $\theta = 0°$, 90° and 180°. Obviously, the

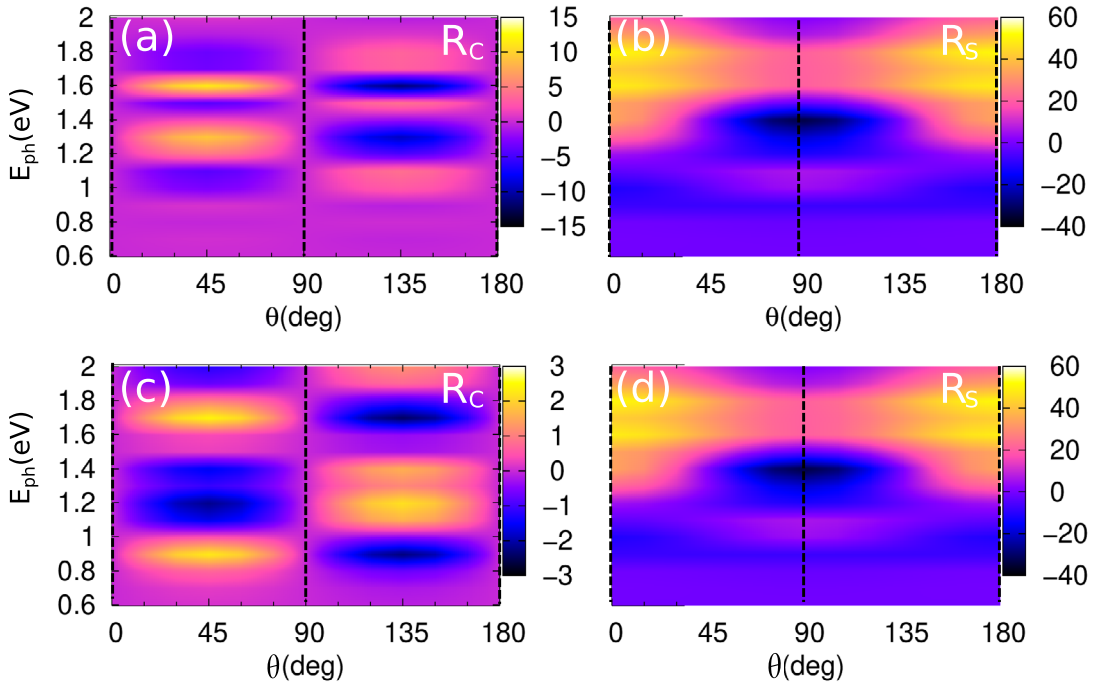

Figure 4. (a) and (c) The total charge photoresponse (R_c) and (b), (d) spin current photoresponse (R_s) versus different polarization/helicity angles in the photon energy range of [0.6,2.0] eV. (a) and (b) are for LPL, while (c) and (d) are for EPL. The black dashed lines denote the angles $\theta = 0°, 90°, 180°$ with pure spin current.

charge photoresponse $R_c = 2a\cos(b)\sin(2\theta)$ still has a sine dependence on 2θ for both LPL and EPL, with zero shift along both horizontal and longitudinal axes. The same features are also observed for other E_{ph} as shown in figures 4(a) and (c), where R_c as a function of both photon energy and polarization/helicity angle is presented and at each energy, a sine relation is obtained for LPL (see figure 4(a)) and EPL (see figure 4(c)).

A very interesting feature found in figure 3(a) is that, for $E_{ph} = 1.0$ eV, $R_\uparrow = 0$ at $\theta = 66.61°$ and $\theta = 132.88°$, which are indicated by A_1 and A_2, and $R_\downarrow = 0$ at $\theta = 47.12°$ and $\theta = 113.39°$, depicted as B_1 and B_2. At these points, only the spin-down or spin-up current is produced by LPL, thus fully spin polarized current can be achieved. Further as shown in figure 3(b) for EPL, there are also four zero points, at which 100% spin polarization can be realized at A_1 and A_2 points for spin-up state and at B_1 and B_2 for spin-down state. It indicates that by tuning the polarization angle of the light, we can switch the spin channels of the photocurrent. Besides $E_{ph} = 1.0$ eV, we have also considered the full spin polarization at other photon energies. Figures 3(c) and (d) show the change of the four points (A_1, A_2, B_1 and B_2) denoting 100% spin polarization with the increase of photon energy for LPL and EPL, respectively. This indicates that, in the energy range [1.0, 1.5] eV, fully spin polarized current can always be generated by tuning the photon energy and selecting certain polarization or helicity angle. This is a direct result of the relative shift of b and c in the expression of $R_\uparrow$ and $R_\downarrow$ as shown in the previous paragraph. We may get the angles $2\theta = -\arcsin(\frac{c}{a}) - b$ and $\pi + \arcsin(\frac{c}{a}) + b$ at which $R_\uparrow = 0$ and $2\theta = \arcsin(\frac{c}{a}) + b$ and $\pi - \arcsin(\frac{c}{a}) - b$ at which $R_\downarrow = 0$, producing fully spin polarized current.

Another striking feature is that $R_\uparrow$ and $R_\downarrow$ always flow in opposite direction and R_c always equals to zero when $\theta = 0°, 90°, 180°$ for both LPL and EPL, indicating pure spin current ($R_s \neq 0$, $R_c = 0$) is produced in our proposed spin photogalvanic device. It is well known that pure spin current plays an important role in spintronics due to its low-dissipation functionality. The robustness of the pure spin current is the basic condition for its practical application. Therefore, the effect of photon energy with a range of [0.6, 2.0] eV is studied. Figures 4(b) and (d) show the sine dependence of R_s on 2θ for both LPL and EPL at any photon energies, which is in good agreement with the features of LPGE and CPGE in previous theoretical and experimental studies [13–15, 18, 20]. Especially, we see that, at each photon energy, $R_c = 0$ and $R_s \neq 0$ always hold when $\theta = 0°, 90°, 180°$ (see figures 4(a)–(d)). It indicates that pure spin current can always be obtained at various photon energies at these polarization/helicity angles.

In order to clearly understand the physical process of the generation of the spin and charge photocurrent and especially, the mechanism of pure spin current at $\theta = 0°, 90°, 180°$ under configuration 'A', we plot two cartoon figures to describe the general process for the proposed device with the mirror symmetry under configuration 'P' and configuration 'A' as shown in figures 5(a) and (b), respectively. Physically, the photocurrent generation process can be divided into three stages [34]: (1) excitation stage: the electrons with energy ε_{in} will be excited from the valence bands below the Fermi level to the empty states with energy $\varepsilon_{out} = \varepsilon_{in} + E_{ph}$ in the conduction bands under the photon irradiation with E_{ph}. (2) Outgoing stage: the excited electrons with energy ε_{out} in the conduction bands will further flow to the corresponding energy state of the left and right leads due to the non-equilibrium between leads and central region induced by the previous photon excitation.

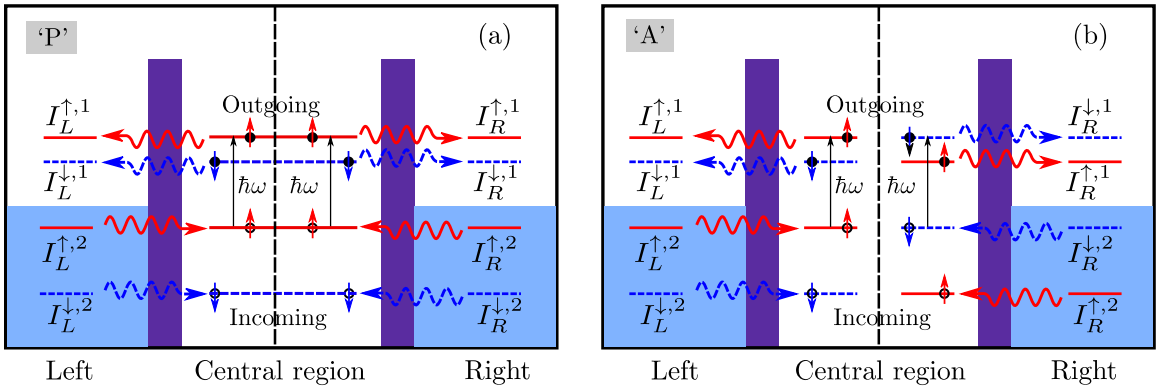

Figure 5. The photocurrent generation process for: (a) configuration 'P' and (b) and configuration 'A'. The red and blue lines denote spin-up and spin-down states, respectively. The black vertical dashed line denotes the mirror reflection plane.

(3) Incoming stage: the electrons with ε_{in} in the leads will be injected to the central region and fill the holes left in the preceding excitation process. The net photocurrent in the leads is determined by the difference of the currents generated in the incoming and outgoing processes. This can be intuitively seen by the effective transmission calculated by (spin index omitted) [34]

$$\begin{aligned} T_{\text{eff},\alpha}(\varepsilon) &= \text{Tr}[\Gamma_\alpha(\varepsilon)G^{>}_{\text{ph}}(\varepsilon)] + \text{Tr}[\Gamma_\alpha(\varepsilon)G^{<}_{\text{ph}}(\varepsilon)] \\ &= T_{\text{eff},\alpha}(\varepsilon<0) + T_{\text{eff},\alpha}(\varepsilon>0), \end{aligned} \tag{5}$$

when the temperature is low enough so that the Fermi distribution is a stepwise function. Here, the first term corresponds to the incoming stage and the second term corresponds to the outgoing stage. For either the incoming stage or the outgoing stage, the photocurrent generated has two contributions which flow left and right, respectively. With the symbols marked in figure 5, in the outgoing stage, the spin-dependent photocurrent $I^\sigma_1 = I^{\sigma,1}_L + I^{\sigma,1}_R$, and in the incoming stage, $I^\sigma_2 = I^{\sigma,2}_L + I^{\sigma,2}_R (\sigma = \uparrow, \downarrow)$. I^σ_1 corresponds to the $\varepsilon > 0$ term while I^σ_2 corresponds to the $\varepsilon < 0$ term in equation (5). The total photocurrent $I^\sigma = I^\sigma_1 + I^\sigma_2$. For a system in the absence of space inversion symmetry where the coupling of the central region and the left lead is not equal to that of the central region and the right lead (that is $\Gamma_L \neq \Gamma_R$), the two contributions in either the incoming stage or the outgoing stage are usually not exactly equal, which means that both the incoming stage and the outgoing stage will contribute to the net photocurrent. Meanwhile, the net photocurrent produced by these two stages will not cancel exactly due to the difference between the valence band and the conduction band. Thus, a total net photocurrent will be produced. However, for a system with space inversion symmetry, $\Gamma_L = \Gamma_R$, which demonstrates that the excited electrons have equal probability of flowing left and right by light illumination and the net total photocurrent in the whole system vanishes.

It can be predicted that photocurrent may be generated by tuning the polarization and helicity angle of the polarized light in a system with C_s symmetry as shown in figures 1(a) and (b) to break the electronic symmetry of the system. When the applied polarized light is linear and the polarization direction is normal ($\theta = 0°$, $180°$) or parallel ($\theta = 90°$) to the mirror reflection plane (denoted as black dash line in figures 1(a) and (b)), C_s symmetry is maintained, thus the left and right coupling satisfies $\Gamma_L = \Gamma_R$ and the net photocurrent in transport direction is zero. This is the reason why the photocurrent vanishes at these special angles under the illumination of the LPL as shown in equation (6). Away from these special polarization angles, the electronic C_s symmetry is broken, which leads to finite photocurrent. For EPL, the similar situation will be observed.

For the two magnetic configurations ('P' and 'A') considered in this work, the tuning effects of the polarization or helicity will be different. Firstly, for configuration 'P' shown in figure 5(a), all of the spin-up, spin-down density distribution and charge distribution maintain mirror symmetry and will not break the C_s symmetry as shown in the inset plot of figure 2(a), thus both $R_\uparrow$ and $R_\downarrow$ are proportional to $\sin(2\theta)$ as shown in figures 2(a) and (b). In contrast, for configuration 'A' shown in figure 5(b), the mirror symmetry is broken for both spin-up and spin-down density distribution as shown in the inset of figure 3(a), thus the spin-dependent photoresponse R_σ is no longer proportional to $\sin(2\theta)$, but in a form of $a\sin(2\theta + b) + c$, indicating that a net photocurrent may be induced for any θ angles including $0°, 90°, 180°$. It is worth noting that, due to the mirror symmetry of the structure and the antiparallel magnetic configuration, on the two sides of the mirror plane, the spin up and spin down electron densities are just simply exchanged. Thus, the sum of them, namely, the total charge density, will be equal at any two sites symmetrical with respect to the mirror plane. Consequently, the total charge density still satisfies the C_s symmetry and the charge current generated by the PGE will still satisfy the $\sin(2\theta)$ relation, behaving in the same way as that in configuration 'P' and even in the NM configuration, namely, R_c is proportional to $\sin(2\theta)$ as shown in figures 3 and 4. Further, since in configuration 'A' the spin-up and spin-down states are antisymmetric with respect to the mirror plane, the flow directions for both the spin-up photocurrent and spin-down photocurrent are always opposite when $\theta = 0°, 90°, 180°$, and their magnitudes are the same, namely, $I^{\uparrow,1}_L = -I^{\downarrow,1}_R$, $I^{\downarrow,1}_L = -I^{\uparrow,1}_R$, $I^{\uparrow,2}_L = -I^{\downarrow,2}_R$, $I^{\downarrow,1}_L = -I^{\uparrow,2}_R$. Furthermore, generally, we have $I^{\uparrow,1}_L \neq I^{\downarrow,1}_L \neq I^{\uparrow,2}_L \neq I^{\downarrow,2}_L$ due to the spin splitting in this system, thus, pure spin current can always be generated at

these angles independent of photon energy. These novel findings originate from the mirror symmetry and anti-symmetric magnetic configuration in the system, and demonstrate that the proposed device with anti-parallel magnetic configuration is a good generator for both fully spin polarized current and pure spin current using PGE.

Finally, we want to note that the photocurrent obtained in this device is consistent with the standard phenomenological theory, [18] which states that, for a material with C_s symmetry, the photocurrent generated by PGE can be expressed by

$$j_z = E_0^2 \chi_{zzx} \sin(2\theta), j_x = E_0^2(\chi_+ + \chi_- \cos(2\theta)) \quad (6)$$

for normally incident LPL, or by

$$j_z = E_0^2 \chi_{zy} \sin(2\theta), j_x = E_0^2(\chi_+ + \chi_- \cos(2\theta)) \quad (7)$$

for normally incident EPL. Here j_z and j_x are the photocurrent along the directions perpendicular and parallel to the mirror reflection plane in the C_s system, respectively. For our proposed 1D H-2H ZSiNRs photoelectric device with C_s symmetry, j_z flows in the transport direction (z axis) in this work. In equations (6) and (7), E_0^2 is the amplitude of the electric field of the polarized light. χ_{zzx}, χ_+, χ_- and χ_{zy} are tensors which depend on the light frequency and temperature. From equations (6) and (7), it is seen that the photocurrent generation is highly related to both material's symmetry and the polarization (helicity) of the polarized light. In the configuration 'P', the electronic structures of both the spin up and spin down channels, such as their charge densities, hold the C_s symmetry, thus both the spin up and spin down photocurrents satisfies the $\sin(\theta)$ relation. In contrast, in configuration 'A', the electronic structure of neither the spin up channel nor the spin down channel holds the C_s symmetry, thus, we cannot get an expression as presented by the j_z in equation (6) or (7). However, since the total charge density is still symmetrical with respect to the mirror plane, the charge current generated by the PGE will satisfy the $\sin(2\theta)$ relation, which is again consistent with the phenomenological theory as shown in the j_z in equation (6) or (7).

4. Summary

In summary, we have designed a H-2H SiNRs-based spin-photovoltaic device, in which asymmetric hydrogenation breaks the space inversion symmetry of pristine silicene nanoribbon and leads to the C_s symmetry. By DFT calculations, it is found that spin-dependent photocurrent can be generated in the proposed device by PGE without the application of an external bias voltage for both parallel and anti-parallel magnetic configurations. For anti-parallel magnetic configuration, a fully spin polarized current can be induced by tuning the polarization (helicity) angle at photon energy [1.0, 1.5] eV, and pure spin current can always be generated when the polarization/helicity angle equals to $0°, 90°, 180°$ by the normal illumination of the LPL/EPL within a wide range of photon energy. These results indicate that 2D FM spin semiconductors are good candidates for producing fully spin polarized photocurrent or pure spin current using PGE and hold great potential for applications in spintronics.

Acknowledgment

The work was supported by the National Natural Science Foundation of China under Grant Nos. 11574318 and 11704232; Shanxi Science and Technology Department (No. 201701D121003) and the Program of State Key Laboratory of Quantum Optics and Quantum Optics Devices (No: KF201810); National Key R&D Program of China under Grants No. 2017YFA0304203; Shanxi Province 100-Plan Talent Program. Calculations were performed in Center for Computational Science of CASHIPS, the ScGrid of Supercomputing Center and Computer Network Information Center of Chinese Academy of Sciences.

ORCID iDs

Peng Jiang https://orcid.org/0000-0002-4291-608X
Xiaohong Zheng https://orcid.org/0000-0002-3027-1042
Lei Zhang https://orcid.org/0000-0002-8634-8037

References

[1] Wolf S, Awschalom D, Buhrman R, Daughton J, Von Molnar S, Roukes M, Chtchelkanova A Y and Treger D 2001 *Science* **294** 1488–95
[2] Žutić I, Fabian J and Das Sarma S 2004 *Rev. Mod. Phys.* **76** 323–410
[3] Awschalom D D and Flatté M E 2007 *Nat. Phys.* **3** 153–9
[4] Vogt P, De Padova P, Quaresima C, Avila J, Frantzeskakis E, Asensio M C, Resta A, Ealet B and Le Lay G 2012 *Phys. Rev. Lett.* **108** 155501
[5] Tsai W F, Huang C Y, Chang T R, Lin H, Jeng H T and Bansil A 2013 *Nat. Commun.* **4** 1500
[6] Le Lay G 2015 *Nat. Nanotechnol.* **10** 202–3
[7] Cahangirov S, Topsakal M, Aktürk E, Şahin H and Ciraci S 2009 *Phys. Rev. Lett.* **102** 236804
[8] Rachel S and Ezawa M 2014 *Phys. Rev.* B **89** 195303
[9] Liu C C, Feng W and Yao Y 2011 *Phys. Rev. Lett.* **107** 2989–96
[10] An X T, Zhang Y Y, Liu J J and Li S S 2012 *Appl. Phys. Lett.* **102** 146802
[11] Zberecki K, Swirkowicz R and Barnaś J 2014 *Phys. Rev.* B **89** 165419
[12] Jiang P, Tao X, Hao H, Song L, Zheng X and Zeng Z 2017 *RSC Adv.* **7** 28124–9
[13] Yuan H, Wang X, Lian B, Zhang H, Fang X, Shen B, Xu G, Xu Y, Zhang S C and Harold Y H 2014 *Nat. Nanotechnol.* **9** 851
[14] Xie Y, Zhang L, Zhu Y, Liu L and Guo H 2015 *Nanotechnology* **26** 455202
[15] Xie Y, Chen M, Wu Z, Hu Y, Wang Y, Wang J and Guo H 2018 *Phys. Rev. Appl.* **10** 034005
[16] Zamani S and Farghadan R 2018 *Phys. Rev. Appl.* **10** 034059
[17] Tao X, Zhang L, Zheng X, Hao H, Wang X, Song L, Zeng Z and Guo H 2018 *Nanoscale* **10** 174–83
[18] Belinicher V I and Sturman B I 1980 *Sov. Phys.—Usp.* **23** 415
[19] Ivchenko E L and Pikus G E 1978 *JETP Lett.* **27** 640

[20] Ganichev S D, Ketterl H, Prettl W, Ivchenko E L and Vorobjev L E 2000 *Appl. Phys. Lett.* **77** 3146–8
[21] Li S, Wang T, Chen X, Lu W, Xie Y and Hu Y 2018 *Nanoscale* **10** 7694–701
[22] Dhara S, Mele E J and Agarwal R 2015 *Science* **349** 726–9
[23] Ding Y and Wang Y 2013 *Appl. Phys. Lett.* **102** 143115
[24] Wang Z F, Jin S and Liu F 2013 *Phys. Rev. Lett.* **111** 096803
[25] Henrickson L E 2002 *J. Appl. Phys.* **91** 6273–81
[26] Chen J, Hu Y and Guo H 2012 *Phys. Rev.* B **85** 155441
[27] Zhang L, Gong K, Chen J, Liu L, Zhu Y, Xiao D and Guo H 2014 *Phys. Rev.* B **90** 195428
[28] Kresse G and Furthmüller J 1996 *Phys. Rev.* B **54** 11169
[29] Kresse G and Joubert D 1999 *Phys. Rev.* B **59** 1758
[30] Blöchl P E 1994 *Phys. Rev.* B **50** 17953
[31] Perdew J P, Burke K and Ernzerhof M 1996 *Phy. Rev. Lett.* **77** 3865–8
[32] Maassen J, Harb M, Michaud-Rioux V, Zhu Y and Guo H 2013 *Proc. IEEE* **101** 518–30
[33] Taylor J, Guo H and Wang J 2001 *Phys. Rev.* B **63** 245407
[34] Chen J, Zhang L, Zhang L, Zheng X, Xiao L, Jia S and Wang J 2018 *Phys. Chem. Chem. Phys.* **20** 26744–51